LASER-INDUCED THERMAL ACOUSTIC MEASUREMENTS IN A HIGHLY BACK-PRESSURED SCRAMJET ISOLATOR MODEL: A RESEARCH PLAN

T. F. Middleton*, R. Jeffrey Balla+, R. A. Baurle*,
NASA, Langley Research Center, Hampton, Virginia

L. G. Wilson*
Lockheed Martin, NASA, Langley Research Center, Hampton, Virginia

ABSTRACT

Under the Propulsion Discipline of NASA's Fundamental Aeronautics Program's Hypersonics Project, a test apparatus, for testing a scramjet isolator model, is being constructed at NASA's Langley Research Center. The test apparatus will incorporate a 1-inch by 2-inch by 15-inch-long scramjet isolator model supplied with 2.1 lbm/sec of unheated dry air through a Mach 2.5 converging-diverging nozzle. The planned research will incorporate progressively more challenging measurement techniques to characterize the flow field within the isolator, concluding with the application of the Laser-Induced Thermal Acoustic (LITA) measurement technique. The primary goal of this research is to use the data acquired to validate Computational Fluid Dynamics (CFD) models employed to characterize the complex flow field of a scramjet isolator. This paper describes the test apparatus being constructed, pre-test CFD simulations, and the LITA measurement technique.

INTRODUCTION

Hypersonic vehicles require a high degree of integration between the propulsion system and the vehicle airframe. The forebody surface of the airframe provides a compression surface, which processes the flow passing through the vehicle's bow shock. In turn, the processed flow captured by the inlet passes into the scramjet isolator. The primary function of the isolator is to deliver a uniform, high-pressure flow to the combustor with minimal aerodynamic losses and to prevent the pressure waves generated in the combustor from propagating upstream into the inlet, potentially causing the inlet to unstart.[1-4] In the combustor, fuel is injected, mixed, and reacted with the high pressure flow exiting the isolator. The reacted flow expands through the scramjet nozzle and along the aftbody of the vehicle's airframe to produce thrust. Figure 1 diagrams the components of a typical propulsion-airframe integrated scramjet and illustrates how the back-pressure from the combustion process causes the boundary layer in the isolator to separate and an oblique shock train to form.

In cold-flow experimental configurations, the combustor pressure is commonly simulated using mechanical means, such as a flow-restricting valve.[5] For a fixed configuration, where the inflow thermodynamic and fluid dynamic properties are constant, the shock pattern that develops in the isolator varies depending on the ratio of the back-pressure (simulated combustor pressure) to the inflow static pressure.[6] For a high ratio, the isolator boundary layer separates and an oblique shock train forms within the isolator. The complex flow field has been investigated both numerically and experimentally; however, the vast majority of the experimental measurements have been limited to wall pressure measurements, stagnation temperature measurements, and Pitot pressure measurements, with a limited amount of nonintrusive measurements, such as shadowgraph and spark schlieren photographty.[7-11]

* Hypersonic Airbreathing Propulsion Branch, MS-168
+ Advance Sensing and Optical Measurement Branch, MS-493

Approved for public release; distribution is unlimited
This Research is Sponsored by the NASA Fundamental Aeronautics Program

The goal of this research is to obtain accurate off-wall measurements of the flow field to validate CFD models that are employed to characterize scramjet isolator flow paths. The selection of the experimental techniques and the development of the research plan have been coordinated with the CFD-model developer's need for accurate off-wall data.[12] While several experimental techniques will be employed, the Laser-Induced Thermal Acoustic (LITA) technique will be the primary focus of this paper.

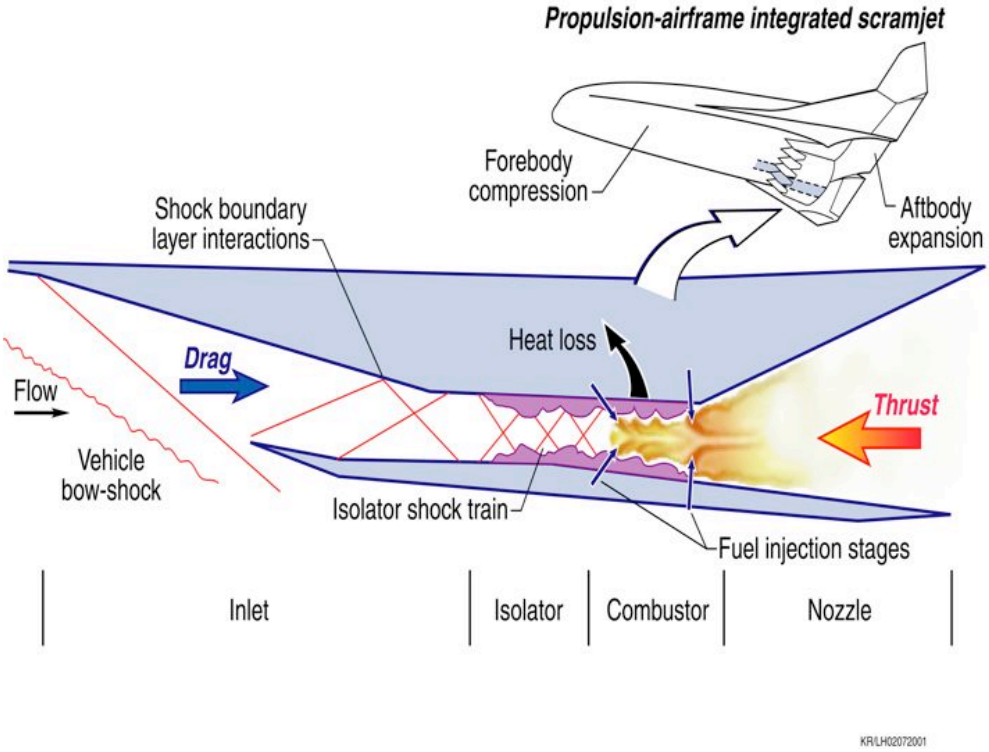

Figure 1. Components of a typical propulsion-airframe integrated scramjet and features of the associated internal flow.

EXPERIMENTAL APPROACH

A sketch of the experimental apparatus is shown in Figure 2, in which unheated dry air will be used as the test medium. To characterize the complex flow within the scramjet isolator; the recovery temperature will be measured using a thermocouple probe, the incipient shock location will be determined from wall pressure taps placed 0.10-inches apart along the top center-line of the isolator, and Pitot pressure measurements will be obtained 1-inch downstream of the nozzle exit for comparison with LITA measurements. Kulite, high frequency transducers, will be placed along the top and bottom walls of the isolator at five axial locations to measure the high frequency pressure fluctuations and assess differences between the fluctuations along the top and bottom walls. The Kulite transducers will be placed at 3-inch intervals starting 1-inch from the nozzle exit. Schlieren or shadowgraph measurements will be made to qualitatively observe the shock train formed in the isolator. Following these measurements Particle Imaging Velocimetry (PIV) and Raman spectroscopy measurements will be incorporated to measure the velocity of the core flow and the velocity profile through the boundary layer for further comparison with the LITA measurements. Table 1 outlines the experimental techniques planned in this experiment.

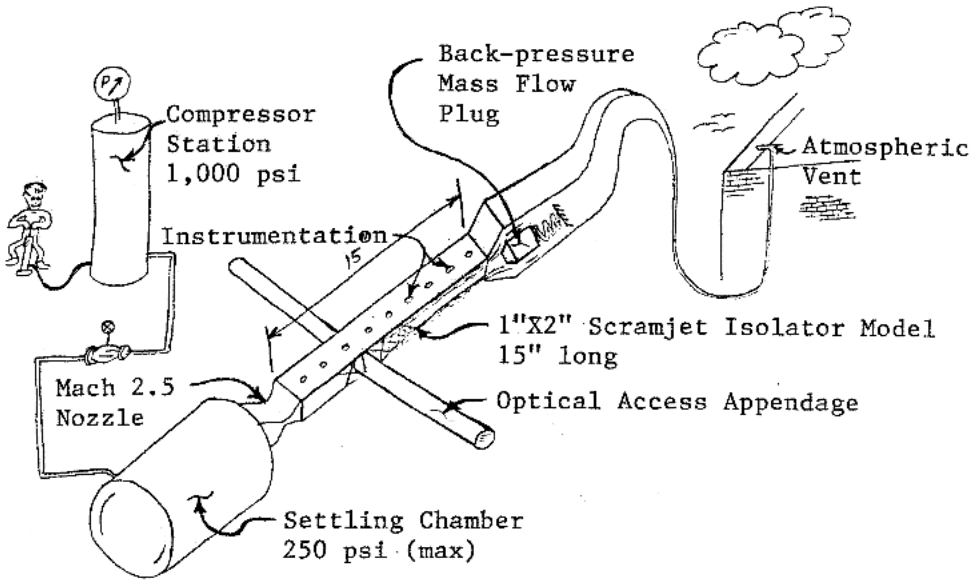

Figure 2. Sketch of Experimental Apparatus.

Sequence	Technique	Parameter	Type	Result
1	Thermocouples Transducers Pitot Probe Kulite	Temperature Wall Pressure Stagnation Pressure High Freq. Pressure	Point Point Point Fluctuation	Recovery Temperature, Shock Location, Pitot Flow Velocity, Unsteady Pressure
2	Schlieren or Shadowgraph	Flow Visualization	Plane	Shock Location
3	Particle Imaging Velocimetry (PIV)	Velocity	Plane	Off-wall Velocity
4	Raman	Rotational Temperature, Density, Pressure	Point	High Resolution Boundary-Layer Measurements
5	Laser-Induced Thermal Acoustics (LITA)	Speed of Sound Temperature Velocity	Local Local 3 Component	Full Mapping of Flow Field, Instantaneous Measurements of Temperature and 3-components of velocity (u, v, & w)

Table 1. Suite of diagnostic measurement techniques to be enlisted in the proposed research.

DESCRIPTION OF THE TEST APPRATUS:

In the isolator, measurements will be made of the local gas temperature, 3-components of velocity, and static pressure. The isolator and supporting test apparatus will be capable of being rotated and translated to acquire, individually, the 3-components of velocity. The air will be supplied from an air compressor station through a 1,000 psi air line and will be reduced to 250 psi (maximum) before being introduced into a 16-inch diameter by 16-inch long settling chamber. The settling chamber will be flange connected to a planar Mach 2.5 converging-diverging nozzle. The nozzle will be mated to a 15-inch-long scramjet isolator model, with a 1-inch by 2-inch constant cross-sectional area. The isolator will be mechanically back-pressured by a conical mass flow plug designed to assure repeatibility of the isolator test conditions. The flow exiting the mechanically back-pressured isolator will exhaust to the atmosphere through a supersonic diffuser. On each side of the isolator, appendages will be attached to provide optical access. A quartz window will be placed at the extremes of the appendages. The opposite ends, adjacent to the isolator, will mate to a slotted wall to allow the focused power of the laser beams access to the internal flow of the isolator. The slots will be 0.08-inches wide and transverse the full vertical height of the isolator (1-inch or 2-inch, depending on the orientation of the model and the component of velocity being measured).

A preliminary contour for the Mach 2.5 nozzle was generated using the, invisid, Method-of-Characteristics (MOC). To account for viscous effects, the nozzle flow field and the exit Mach number profile were then resolved using the Full Navier-Stokes (FNS) solver, Viscous Upwind aLgorithm for Complex flow ANalysis (VULCAN).[13] Comparing the MOC solution with the FNS solution, a new exit Mach number was selected and the MOC reapplied to generate a new nozzle contour. The flow field was again resolved for the new nozzle contour using the FNS solver. This process was repeated until the percent difference in the exit core-flow Mach number profile varied by less than 0.2%. The Mach contours of the final design are shown in Figure 3. The exit Mach number and static pressure profiles from the final FNS solution are shown in Figure 4.

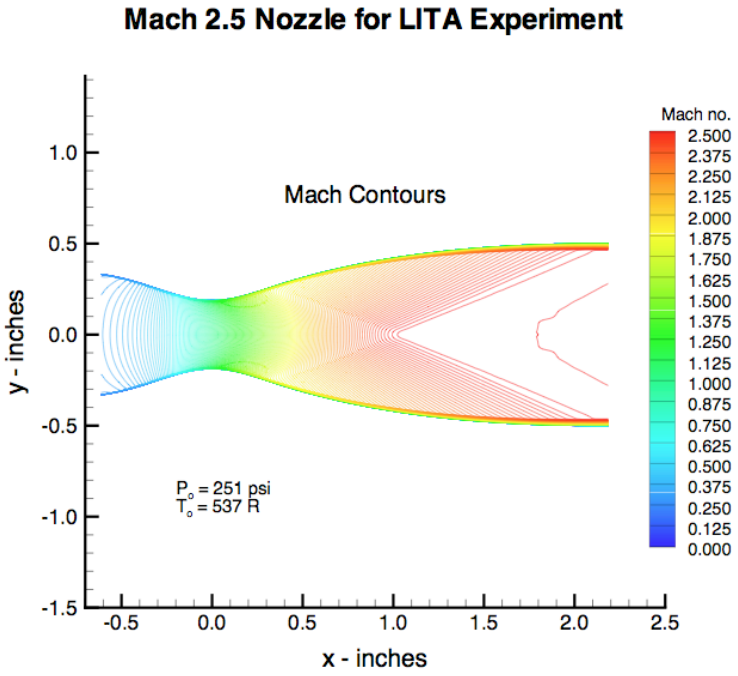

Figure 3. Mach contours for a planer Mach 2.5 nozzle designed for the LITA isolator experiment.

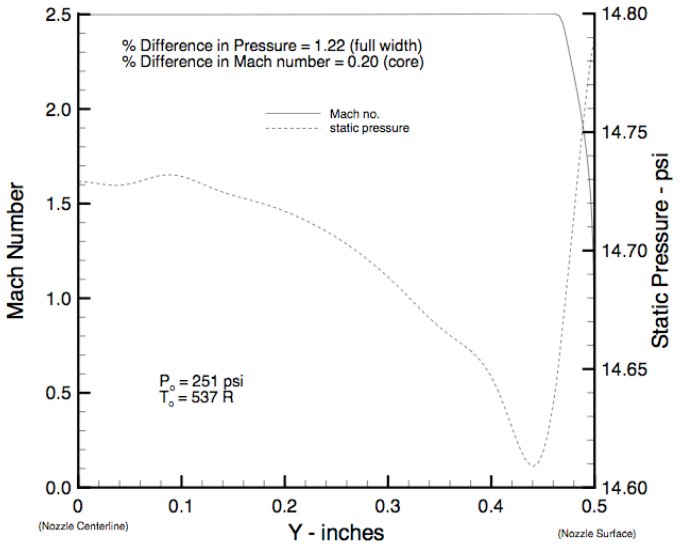

Figure 4. Mach number (left scale) and static pressure (right scale) profiles at exit of Mach 2.5 nozzle.

PRE-TEST CFD SIMULATIONS:

Pre-test CFD simulations were conducted to investigate parameters that could be experimentally controlled, if necessary, to improve the quality of the data set. Four parameters were modeled independently. The parameters considered were temperature, turbulence intensity, supply pressure, and the ratio of the supply pressure to the back-pressure (simulated combustor pressure). The pre-test simulations were performed using a two-dimensional computational model; therefore, sidewall effects have been neglected. The computational domain extended from the facility nozzle to the exit of the isolator. These simulations were run for a 10-inch isolator as shown in Figure 5; however, in order to capture the maximum pressure rise in the isolator, the isolator length was increased to 15-inches during the conceptual design phase. The revised length does not effect the conclusions drawn from this simulation.

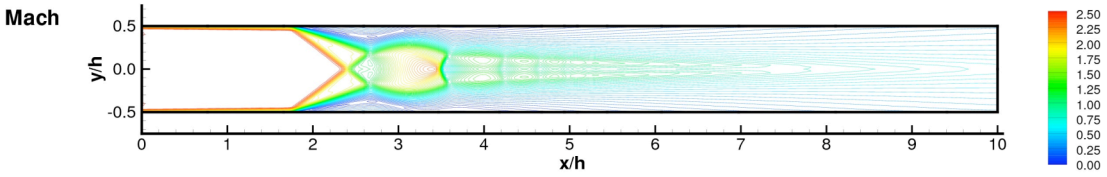

Figure 5. CFD solution of Mach contours of baseline condition.

Five cases were simulated to examine the sensitivity of the solution to pressure, temperature, and turbulence intensity. The back-pressure was set to 99.35 psi (approximately 95% the normal shock value) to model what is expected to be the worst-case scenario with regards to flow field sensitivities. The details of these cases are given in Table 2. Case 0 represents the baseline condition, and cases 1-4 involve perturbations of a single parameter from this baseline condition. Case 1 considers the effect of increasing the inflow turbulence intensity by a factor of 500. Case 2 considers the effect of reducing the supply temperature from a typical summer month value to a

typical winter month value. Case 3 considers the effect of a supply pressure variability of approximately 1.5% with the applied back-pressure held constant, while Case 4 considers the effect of the supply pressure and back-pressure variability where the ratio of these pressures is held constant.

Case	Input Parameters				Results			
	P_o [psi]	T_o [R]	Turbulence Intensity	P_o/P_b	Mach No.	P [psi]	C_f	X_s/h
0	250.00	536.67	0.0001	2.51635	2.475	14.6011	1.831e-3	1.6920
1	250.00	536.67	0.0500	2.51635	2.475	14.5974	1.829e-3	1.6588
2	250.00	549.67	0.0001	2.51635	2.475	14.5567	1.807e-3	1.7252
3	246.25	536.67	0.0001	2.47860	2.475	14.3819	1.830e-3	N/A
4	246.25	536.67	0.0001	2.51635	2.475	14.3819	1.830e-3	1.6920

Definition of terms used in Table 2:

P_0 = Total pressure, psi
T_0 = Total temperature, R
P_b = Back-pressure (simulated combustor pressure), psi
P = Inflow static pressure, psi
C_f = Skin friction coefficient
X_s = Axial location measured from the nozzle exit (inch)
H = Height of isolator, 1 inch (2-Dimensional simulation)

Table 2. Results of CFD simulations.

All simulations were performed using the VULCAN Navier-Stokes code. The results were obtained by integrating the Reynolds-Averaged Navier-Stokes equations in a fully elliptic fashion. The inviscid fluxes were evaluated using the Low-Diffusion Flux Split Scheme (LDFSS) of Edwards.[14] The MUSCL (Monotone Upwind Schemes for Conservation Laws) extrapolation parameter κ was chosen as 1/3 to minimize spatial truncation error, and the van Leer flux limiter was employed to enforce Total Variation Diminishing (TVD). All of the steady-state solutions were advanced in time using an Incomplete LU (ILU) scheme with a Courant number (CFL) of 5000. The turbulence model chosen was the Wilcox (1998) k-ω model,[15] and the wall function procedure of Wilcox[16] was used to relax the grid spacing requirements near solid surfaces. The walls were assumed as adiabatic surfaces, and a turbulent Prandtl Number (Pr_t) of 0.9 was used in all of the simulations. All calculations were considered converged when the L2 norm of the residual error was reduced by 8 orders of magnitude.

The result of increasing the inflow turbulence intensity, Case 1, by a factor of 500 had a negligible effect on the shock train position. The reduction in supply temperature, Case 2, also had a negligible impact on the shock train position. The largest deviation from the baseline condition occurred for Case 3, where the supply pressure was reduced by 1.5% while maintaining a constant back-pressure at the exit of the isolator. The shock system that resulted from this case

extended several duct heights upstream of the baseline condition and settled in the facility nozzle. If the back-pressure is adjusted such that the back pressure to plenum pressure ratio matches that of the baseline condition, Case 4, then the shock train collapses back to what was observed for the baseline case. The wall pressure distribution for each case is shown in Figure 6.

The results of this study indicate, to maintain a constant incipient shock location, care must be taken when setting facility pressure values, such that the back-pressure to plenum pressure ratio is maintained at a constant value. This is particularly important when employing the LITA measurement technique, since data gathered at different axial stations and/or on different days will be compile to represent one mapping of the flow field at a given “nominal” test point

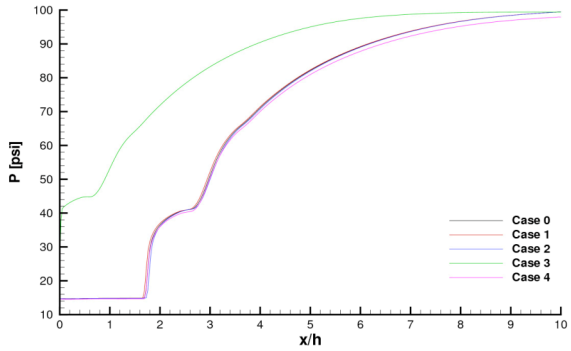

Figure 6. Wall pressure distributions for each of five cases simulated.

Since the isolator portion of the test apparatus is required to have slotted walls to provide optical access, appendages will be mounted on each side wall, with one end open to the isolator flow field through a wall slot and the other end sealed around a quartz window. To investigate the effects that the slots may have on the isolator’s flow field, an additional simulation was run. The configuration and resulting pressure profiles at three stations and wall pressure distributions are shown in Figure 7. The results show negligible difference in the pressure profiles at the three stations and negligible difference in the wall pressure distributions for simulations run with, and without, the simulated slots.

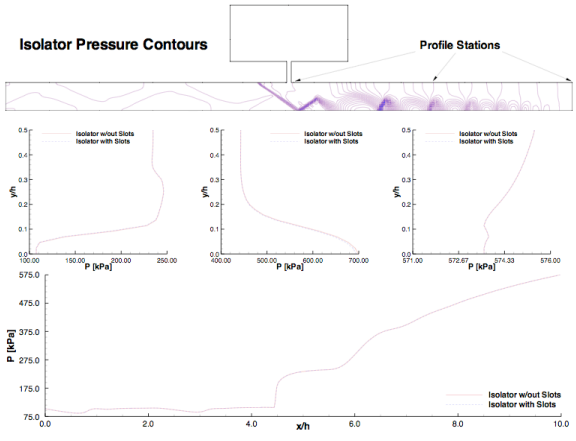

Figure 7. CFD calculations of shock train; pressure profiles at three stations; and wall pressure distributions with, and without, wall slots.

LASER-INDUCED THERMAL ACOUSTIC MEASUREMENT TECHNIQUE:

Interest in the application of the LITA measurement technique is derived from its capability to make high accuracy measurements of temperature,[17] speed of sound,[18] and velocity[19] during a single laser pulse.

LITA differs from spectroscopic techniques in the way temperature and other gas properties are obtained from the laser signal. In spectroscopic techniques, temperature of a single specie, within the gas mixture, is determined by measuring the energy levels in the rotational-vibrational populated states and then fitting a Boltzmann distribution function to deduce the temperature.[20] LITA measures bulk fluid properties directly by a two step process in which a short duration pump laser is used to introduce an acoustic wave in the gas, and then the speed at which the acoustic wave propagates is measured using a continuous wave (cw) probe laser.[21] Knowing the composition of the gas, the local temperature can be deduced from the measured speed of sound using well established relationships for the speed of sound as a function of temperature (see Appendix A of Reference 17).

A description of the theory behind LITA is presented in Reference 21 and a typical experimental configuration is shown in Figure 8. In the first step, the beam from the high-peak-power pulsed (10 ns) pump laser is split into two beams and crossed at a small angle, typically 1 degree. At the focus, the resulting interference pattern creates two counter propagating acoustic waves by electrostriction.[22] As the acoustic waves counter propagate, they interfere constructively and destructively. The maximum dimension of the ellipsoidal sample volume, normal to the interference fringes, is on the order of 1-mm and the dimension parallel to the interference fringes is on the order of 10-mm. In the proposed research, measurements will be made at five axial locations starting at 1-inch downstream of the nozzle exit. The facility will be rotated and translated, such that approximately 50 points at each axial location will be interrogated.

In the second step, the continuous wave laser beam is Bragg scattered off the acoustic waves. The temporal resolution of the LITA measurement is defined by the attenuation of the acoustic wave and is on the order of several hundred nanoseconds as shown in Figure 9. The Bragg scattering creates an intensity modulation in the scattered laser light at a frequency (~20 MHz) twice that of the counter propagating acoustic waves (~10 MHz). This frequency can be related to the local speed of sound in the gas. These acoustic waves rapidly decay by acoustic absorption; hence, signals reflect the intensity modulation of the counter propagating acoustic waves convolved with a damping function created by acoustic absorption. Resulting waveforms resemble damped sinusoidal functions. A typical output is shown in Figure 10 for two different temperatures.

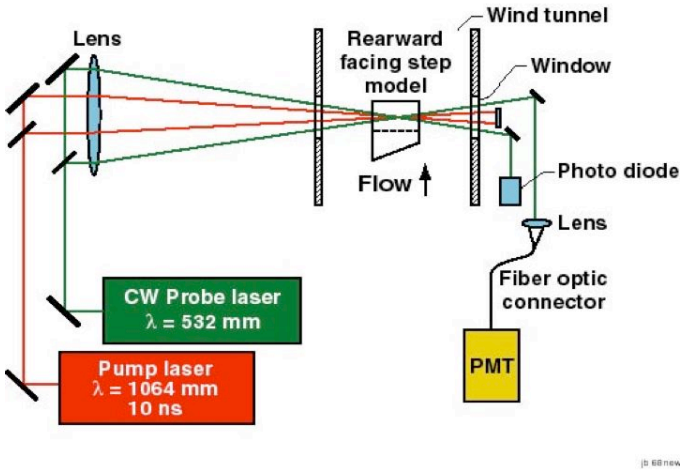

Figure 8. Typical LITA experimental configuration.

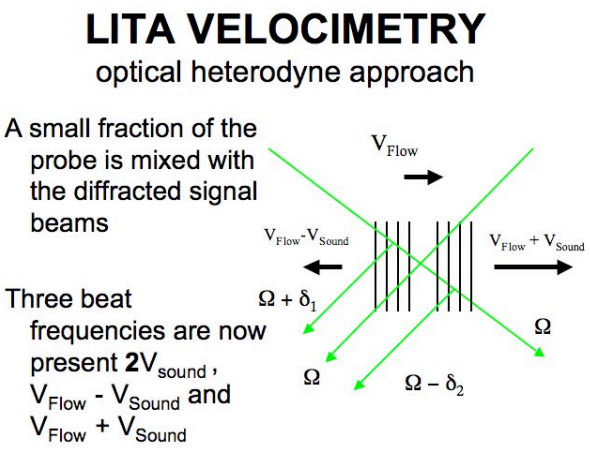

Definition of terms used in Figure 9:

V = Velocity, m/s
Ω = Frequency of Probe Laser
δ = Doppler frequency shift
Ω ± δ = Beat frequencies

Figure 9. Interference grating and Bragg scattered beam.

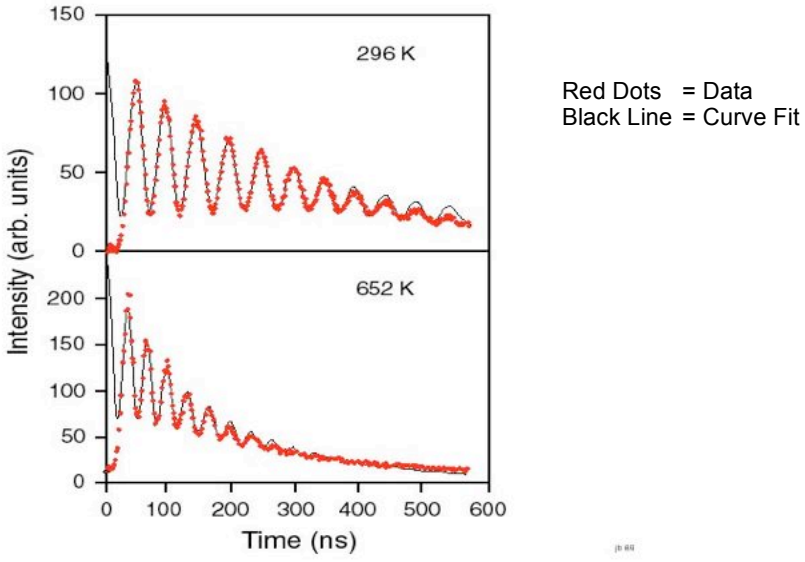

Figure 10. Representative LITA output signals for deducing the local speed of sound.

LITA has been applied successfully to measure the local speed of sound in air within the temperature range from 300 K to 650 K, [17] and previously, with a slightly different configuration at temperatures up to 1370 K.[22] In Figure 11, the temperatures measured using the LITA technique are compared with thermocouple measurements and found to agree within 1%.

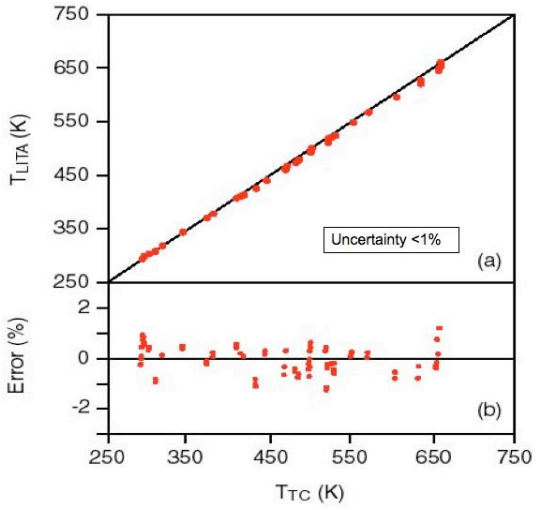

Figure 11. Comparison of temperatures measured using the LITA technique to temperatures measured with a thermocouple.

SUMMARY AND CONCLUSIONS

The work proposed in this research plan is ongoing and is sponsored by NASA's Fundamental Aeronautics Program. Off-wall measurements of temperature, pressure, and 3-components of velocity will be used to validate the CFD models employed to characterize the flow field in scramjet isolators. This research presents a new application challenge for LITA and will be the first attempt to apply LITA in a high Mach number (Mach 2.5), low temperature (135K) environment. Advantages inherent to LITA are its temporal resolution (~ 600 nanoseconds), its spatial resolution (~ 1 X 10 mm, ellipsoidal volume), and it does not require seeding the flow to obtain velocity measurements. Previous LITA measurements of temperature and velocity agree well with conventional thermocouple measurements and velocity measurements obtained from Pitot pressure measurements, respectively.

ACKNOWLEDGMENTS

Writing is a learning experience, and I would like to thank my co-authors for their commitment to this research effort and for sharing with me their knowledge of LITA experimental techniques, keys to good numerical simulations, and expertise in facility engineering.

REFERENCES

1. Reintarz, B. U.; Herrmann, C. D.; Ballmann, J.: ***Aerodynamic Performance Analysis of a Hypersonic Inlet Isolator Using Computation and Experiment.*** Journal of Propulsion and Power, Vol. 19, No. 5 (2003)
2. Auslender, A. H.: ***An Analytic Performance Investigation of Mechanically Back-Pressured Ramjet Data.*** JANNAF 34th, October 27-31 (1997)
3. Rice, T.: ***High Aspect Ratio Isolator Performance for Access-to-Space Vehicles.*** AIAA 2003-7041 (2003)

4. Emami, S; Trexler, C. A.; Auslender, A. H.; Weidner, J. P.: ***Experimental Investigation of Inlet-Combustor Isolators for a Dual-Mode Scramjet at a Mach Number of 4.*** NASA Technical Paper 3502 (1995)
5. Hass, M; Karanian, A. J.: ***Small-Scale Supersonic Inlet Test Facility.*** AIAA (1980)
6. Lin, P.; Rao, G. V. R.; O'Connor, G. M.: ***Numerical Analysis of Normal Shock Train in a Constant Area Isolator.*** AIAA 91-2162 (1991)
7. Waltrup, P. J.; Billig, F. S.: ***Structure of Shock Waves in Cylindrical Ducts.*** AIAA Vol. 11, No. 10, October (1973)
8. Sullins, G.: ***Experimental Results of Shock Trains in Rectangular Ducts.*** AIAA 92-5103 (1992)
9. Wang, C. P.; Zhang, K. Y.; Yang, J. J.: ***Analysis of Flows in Scramjet Isolator Combined with Hypersonic Inlet.*** Presented at AIAA meeting, January 10-13, 2005, Reno Nevada (2005)
10. Carroll, B. F.; Dutton, J. C.: ***Characteristics of Multiple Shock Wave/Turbulent Boundary-Layer Interactions in Rectangular Ducts.*** J. Propulsion, Vol. 6, No. 2 (1990)
11. Kumar, A.; Balu, G.; Panneerselvam, S.; Rathakrishnan, E.: ***Performance of an Isolator Fed with Parallel Flow.*** Presented at AIAA meeting, July 10-13, 2005, Tucson, Arizona (2005)
12. Gaffney, R. L. Jr.; Cutler, A. D.: ***CFD Modeling Needs and What Makes a Good Supersonic Combustion Validation Experiment.*** Presented at the JANNAF Conference, Charleston, SC, June (2005)
13. Baurle, R. A. (web site Curator): http://vulcan-cfd.larc.nasa.gov
14. Edwards, J. R.: ***A Low Diffusion Flux-Splitting Scheme for Navier-Stokes Calculations.*** Computers and Fluids, Vol. 26, No. 6, 635-659 (1997)
15. Wilcox, D. C.: ***Turbulence Modeling for CFD.*** DCW Industries, Inc. Edition 2nd, (1998)
16. Wilcox, D. C.: ***Wall Matching, a Rational Alternative to Wall Functions.*** AIAA 89-0611, January (1989)
17. Hart, R. C.; Balla, R. J.; Herring, G. C.: ***Non-resonant Referenced LITA Thermometry in Air.*** Applied Optics, 38, 577-584 (1999)
18. Hart, R. C.; Balla, R. J.; Herring, G. C.: ***Optical Measurement of the Speed-of-Sound in Air Over the Temperature Range 300-650K.*** The Journal of Acoustical Society of America, 108, 1946-1948 (2000)
19. Hart, R. C.; Balla, R. J.; Herring, G. C.: ***Simultaneous Velocimetry and Thermometry of Air by Use of Nonresonant Heterodyned Laser-Induced Thermal Acoustics.*** Applied Optics, 40, 965-968 (2001)
20. Eckbreth, A. C.: **Laser Diagnostics for Combustion and Species**, Volume 7, Energy and Engineering Science Series: Abacus Press, (1988)
21. Cummings, E. B.: ***Laser Induced Thermal Acoustics.*** PhD Thesis, California Institute of Technology, Pasadena, California (1995)
22. Stampanoni-Panariello, A.; Hemmerling, B.; Hubschmid, W.: ***Temperature Measurements in gases using laser-induced electrostrictive gratings.*** Springer-Verlag: Applied Physics B, Laser and Optics (1998)